CHEMICAL ENGINEERING TRANSACTIONS
VOL. 94, 2022
A publication of AIDIC
The Italian Association of Chemical Engineering
Online at www.cetjournal.it
Guest Editors: Petar S. Varbanov, Yee Van Fan, Jiří J. Klemeš, Sandro Nižetić

ISBN 978-88-95608-93-8; **ISSN** 2283-9216
DOI: 10.3303/CET2294121

Experimental Testing for Calcium Carbonate Nanoparticles Production in a Rotating Packed Bed

Evie Nessi[a,b], Marianthi Dimoliani[a], Athanasios I. Papadopoulos[a,*], Gianna Ntourou[a], Spyridon Voutetakis[a], Konstantinos Intzes[c], George Dimitriadis[c], Panos Seferlis[a,b]

[a]Chemical Process and Energy Resources Institute, Centre for Research and Technology-Hellas, 57001 Thermi, Greece
[b]Department of Mechanical Engineering, Aristotle University of Thessaloniki, 54124 Thessaloniki, Greece
[c]CaO Hellas, Thessaloniki, 56429, Greece
spapadopoulos@certh.gr

In this work a pilot plant with a rotating packed bed (RPB) reactor for nanoparticle production is demonstrated. The overall process is explained and the preliminary experimental outcomes are interpreted. The experiments are performed with slacked lime suspensions and CO_2 gas. Three crucial process parameters, namely rotating speed, slurry flow and gas flow rate, were studied for their impact on the process key performance indicators (KPIs) of reaction time (t_{rxn}), particle size ($\bar{d}$) and capture efficiency (ΔCO_2). A factorial design with three factors and two levels was employed in order to attain a generalized view of the process behavioral trends. The reaction time was derived from pH measurements. Products were characterized by X-ray diffraction, scanning electron microscopy and particle size distribution measurement methods. Capture efficiency was estimated through gas flow rate measurements. The results indicated the successful production of nano-sized calcite particles with diameters down to 34 nm.

1. Introduction

Quicklime (CaO) industry is amongst heavy CO_2 emitters and in great need for capture technologies, since CaO production leads to almost equal emissions of CO_2 by-product. A viable solution is to recycle the captured CO_2 as a raw material in a Rotating Pack Bed (RPB) reactor for the production of value-added products like carbonate nanoparticles, in this case $CaCO_3$. Nanoparticles are gaining attention thanks to their numerous emerging applications. Carbonate nanoparticles are appreciated for the favourable properties that they bring in nanocomposite materials where they are employed (Jimoh et al., 2018). Their mass scale production mainly follows liquid phase methods with a bottom-up approach. Synthesis is commonly performed in continuous stirred reactors (CSTRs) under agitation or bubble reactors that have typical intrinsic shortcomings like large equipment sizes, long processing times and poor controllability over the product characteristics, i.e. particle size distribution, morphology and other (Jimoh et al., 2018). Due to these shortcomings, harsh synthesis conditions are mandatory, like very high gas pressures (Onn et al., 2019) and concentrated corrosive acids (Chen et al., 2020), that incur detrimental environmental impacts due to heavy energy usage and pollution. For the same reasons, crystal growth inhibitors and other additives are a sine qua non in most studies (Wang et al., 2004).
RPB reactors enable process intensification for CO_2 capture and utilisation, offering important advantages, that have been reported through modelling (Dimoliani et al., 2021) and experimental (Emami-Meibodi et al., 2018) studies. The centrifugal forces that develop in an RPB lead to the formation of thin liquid films and droplets, enabling significant intensification of micromixing and mass transfer rates, thus achieving rapid nucleation and relatively even spatial concentration (Kang et al., 2018). As a result, precise controllability of particle size and distribution can be achieved. RPBs find some industrial applications (Neumann et al., 2018) including commercial preparation of $CaCO_3$ nanoparticles (Chen et al., 2000), but the overall details of the process remain undisclosed. Lately studies pursue the synthesis of $CaCO_3$ while recycling industrial by-products or waste streams, like CO_2, as feedstock. Sun et al. (2011), synthesized nano-$CaCO_3$ of 10–80 nm by NH_3/CO_2

Paper Received: 16 April 2022; Revised: 05 May 2022; Accepted: 17 May 2022
Please cite this article as: Nessi E., Dimoliani M., Papadopoulos A.I., Ntourou G., Voutetakis S., Intzes K., Dimitriadis G., Seferlis P., 2022, Experimental Testing for Calcium Carbonate Nanoparticles Production in a Rotating Packed Bed, Chemical Engineering Transactions, 94, 727-732 DOI:10.3303/CET2294121

absorption in $CaCl_2$ solution at low temperature, thus with a need of extra utilities for cooling. Chang et al. (2012) who carbonated steelmaking slags, focused on process optimisation and dealt less with particle size/morphology. Emami-Meibodi et al. (2018) validated experimentally a process model and obtained $CaCO_3$ with a rather broad particle size distribution (PSD) in the range of 24-5,000 nm by applying very high rotating speeds (≥ 3000 rpm). Chen et al. (2020) carbonated calcium-containing industrial wastewater and obtained larger primary particles (>5 μm) of low purity. These provide the state of play for the current experimental study, which pertains to the investigation for $CaCO_3$ nanoparticles production in a RPB pilot-scale setup, where a waste stream of CO_2 is utilized. Here, the carbonation is performed at mild conditions of temperature and pressure, excluding the use of corrosive leaching agents and size/morphology controlling additives.

2. Experimental

2.1 Process description

A circular slurry carbonation method is applied as shown in Figure 1. The slacked lime ($Ca(OH)_2$) slurry is pumped from the "reactant tank" to the RPB and is introduced to the center of the doughnut-shaped packing. The slurry spreads radially on the rotating packing forming thin films and droplets. The CO_2 gas is introduced in co-current mode. and reacts with the slurry on the packing. The unreacted gas exits the RPB casing and is quantified, while the slurry flows into the "product tank". From there it is recycled into the "reactant tank" and is continuously circulated until complete conversion of $Ca(OH)_2$ marked by pH neutralization-. Sampling points are denoted as (1), (2) and (3) in the flowsheet of Figure 1.

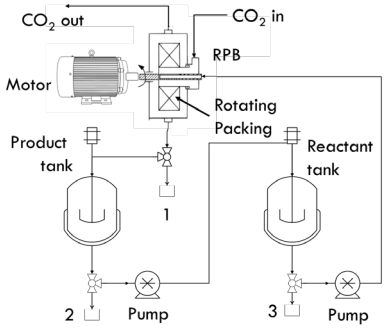

Figure 1. Simplified process flow sheet of RPB pilot plant for the production of $CaCO_3$ nanoparticles

2.2 Materials and methods

Two types of precursors were tested. One simple $Ca(OH)_2$ powder (93 % purity, d_{50} of 88.64 μm, SSA of 14.5 m^2/g) and a $Ca(OH)_2$ powder with elevated specific surface area (SSA) (33.4 m^2/g), herein denoted as "$Ca(OH)_2$+". Slacked lime slurry was prepared in deionised water (30 L) and loaded in the pilot plant. The slurry was heated and circulated in the system under N_2 flow until it reached the desired reaction temperature. Then CO_2 feed was initiated. CO_2 dissolved in the aqueous media and reacted with dissociated calcium ions, producing $CaCO_3$ embryos which grew under the influence of heat and time. The reaction progress was monitored by off-line pH measurement (Metrohm 906 Titrando). Over time the pH was reduced from 12 to 6.5, indicating completion of the reaction. Product samples were collected, then filtrated, rinsed and air-dried overnight at 105 °C. X-Ray diffraction analysis was used for structure identification (BRUKER/D8 Advance D8 Advance Diffractometer, Cu K_α radiation, scanning range 5-80°/0.04°). The crystallite size was calculated based on the Debye-Scherrer equation. The purity was specified by thermogravimetry (TGA) (LECO TGA 701, 0-960°C). The product powder was re-suspended in water for secondary PSD analysis (Laser Scattering Particle Size Distribution Analyzer LA-960/HORIBA). The morphology was observed by scanning electron microscopy (SEM), (JEOL 6300, Oxford ISIS-2000), and the primary particle size distribution was measured through the opensource tool Image J®. Based on existing literature, the initial solid concentration, gas and slurry flow rate, L/G ratio and rotating speed were identified as the most crucial parameters (Sun et al.,2011). The process performance was evaluated by three key performance indicators (KPIs): i) reaction (processing) time for complete consumption of $Ca(OH)_2$ ii) particle size and iii) CO_2 capture efficiency of the pilot plant reactor (Eq(1)). Thus, various operating conditions were assessed for their effect on the KPIs (Table 1).

$$\Delta CO_2 = \frac{m^{in}_{total\ CO_2} - m^{out}_{total\ CO_2}}{m^{in}_{total\ CO_2}} \times 100\ [\%] \quad (1)$$

Table 1. Range of operating conditions studied. P stands for product $Ca(OH)_2$+precursor, S stands for product of the $Ca(OH)_2$ precursor

Products	Precursor	Initial solids (g/L)	V_g (L/min)	V_{sl} (L/min)	Rotating speed (rpm)	T_{rxn} (°C)
P-1 to P-4	$Ca(OH)_2$+	10	3	3.43-4.75	1000	50 - 55
S-1 to S-28	$Ca(OH)_2$	10,30,50	3,6	3.43-4.75	600,1000, 1800	50 - 55; 60 - 65

3. Results and Discussion

Calcite was identified as the main phase for all synthesised materials (JCPDS:5-586) regardless of the precursor. A secondary phase called “beta-calcite” was identified only in sample S-28, which is a calcite polymorph. Final product purities ranged between 97.6 - 98.14 %. Loss on ignition (LOI) values calculated via TGA were lower than the theoretical for pure $CaCO_3$ indicating the presence of species that do not further decompose. It is likely that small amounts of unreacted $Ca(OH)_2$ exist at concentrations lower than the detection limits of the X-RD device. $Ca(OH)_2$ is likely converted to CaO by losing its lattice water up to 400 °C. CaO does not further decompose and remains as an impurity. SEM images reveal submicron clustered particles appearing as aggregates of primary crystals. The derived morphology coincides with the one anticipated for $CaCO_3$ (Figure 2). Some are arranged in a chain-like morphology, typical for calcium carbonate (Coltelli et al., 2018).

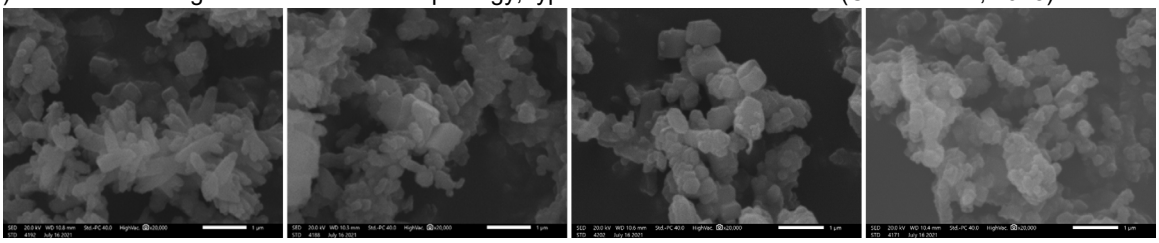

(a) (b) (c) (d)

Figure 2. Representative RPB products: a-b) S-1, S-4 (precursor: simple $Ca(OH)_2$) and c-d) P1-P4 (precursor: Ca(OH)2+). Magnification: ×20.000. Space bar: 1 μm

3.1 Effect of operating parameters on reaction time

Preliminary testing was performed with dilute slurries (10g/L) to eliminate the collateral effects of high viscosity, for two precursors at 1000 rpm. The increase of the slurry flow rate was beneficial for the reaction time when the simple SSA precursor was employed (Figure 3c), while no noteworthy effect was recorded for the elevated SSA precursor. The reaction rates for the latter showed a higher reactivity.

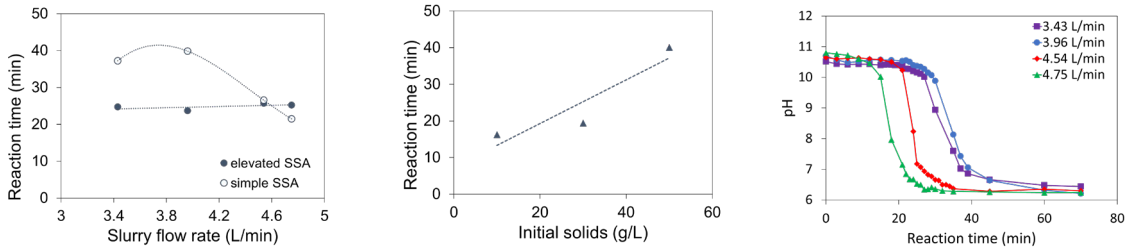

(a) (b) (c)

Figure 3. Initial testing results with reaction time depending on: a) Slurry flow rate (L/min) and precursor type, b) Initial concentration (g/L) at 1000 rpm, c) pH monitoring (reaction time calculation error: ± 0.29 min, pH measurement error ± 0.003)

Precursors of lower grade can achieve reaction times similar to their refined counterparts, thanks to the intensified mass transfer conditions provided by the RPB (Figure 3a). Thus, the study continued with the simple SSA precursor. Similar tests were performed for denser slurries. The reaction time increased linearly with the initial concentration (Figure 3b). This pattern was also observed in other studies (Chen et al., 2000). Thus, for simplicity, slurries of 30 g/L were selected to proceed for pilot plant validation at reaction temperature of 60 °C. The KPI response was observed by studying the effect of three independent parameters (rotating speed – slurry – gas flow rate) at two levels – low (600rpm, 3 L CO_2/min – 3.43 L slurry/min) and high (1,800 rpm – 6 L CO_2/min – 4.75 L slurry/min). This parametric study indicated that when two out of three operating parameters were set

at the low level, then the increase of the third increased the reaction time in all occasions. When two out of three were set at the high level, increasing the third was either beneficial for the reaction time or neutral. The increase of the rotating speed, when the gas and slurry were set at the low level, increased the reaction time by 26.7 %, whereas it contributed to a 14.6 % decrease, when the other parameters were at the high level (Figure 4a). Increasing the slurry flow rate contributed to 36.5 % increased reaction time when the rotating speed and gas flow rate were low, while it had no significant effect when the they were set at high level (Figure 4b).

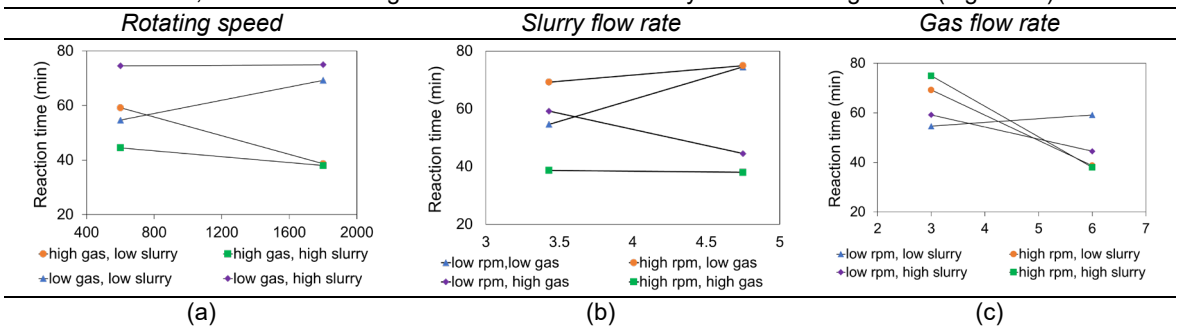

Figure 4. Reaction time (min) response incurred by variation of a) rotating speed, b) slurry, and c) gas flow. Low level: gas 3 L/min, slurry 3.43 L/min, rotating speed: 600 rpm. High level: gas 6 L/min, slurry 4.75 L/min, rotating speed: 1800 rpm (reaction time calculation error: ± 0.29 min)

The increase of the gas flow rate increased the reaction time by 8.3 % when the slurry and speed were low, but contributed to a significant decrease of 49.3 % when the other parameters were already set at high level (Figure 4c). A transient behaviour was observed for all the other combinations of operating parameters. Pursuant to the above, in order to minimise the reaction time, a combination of high rotating speed with high slurry flow rate and lower gas flow rate seemed beneficial.

3.2 Effect of operating parameters on particle size

PSD analysis showed secondary particle sizes (clustered primary particles) of 2.5-3.5 μm. The size of 30 primary particles per sample was measured through Image J analysis (Figure 2a). These data were used to extract distribution curves for the calculation of the mean particle size of the primary particle (Figure 5b,c). All particles lied within a range of 181 - 443 nm (Figure 5a), constituted of nano-crystallites of average size of 49.7 nm.

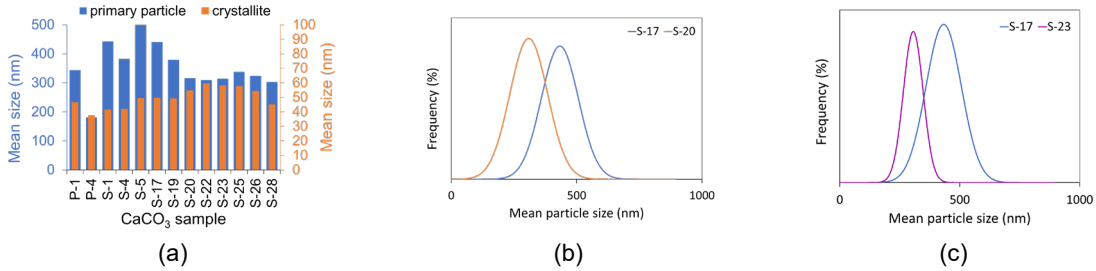

Figure 5. Representative primary particle and crystallite a) sizes (nm), b) PSD where the size reduction is induced by the change of the slurry flow rate (L/min), and c) PSD where the size reduction is induced by the change of the gas flow rate (L/min) (The primary particle size measurement error is introduced by the user of the Image J software and is random. The crystallite size measurement error is automatically corrected by the XRD instrument).

An effect-response study was performed to derive operating trends. The response trends were similar to those of the reaction time. Figure 6 indicates that when two out of three parameters were set at the low level, the increase of the third one reduced the particle size. Among them the slurry flow rate, whose 27 % variation induced a 28% reduction in the particle size, seems to be the most significant, whereas to achieve a similar reduction of particle size, the gas flow rate must be doubled. When two out of three parameters were set to the high level, the variation of the third one does not alter the particle size (line parallel to the x-axis). This was likely due to the extremely short residence time of the gas or the slurry in the RPB, such that a measurable effect could not be quantified. Alternatively, it could be attributed to poorly wetted packing, caused by out-of-limits operation, often visible by entrainment. The Debye-Scherrer equation gave a crystallite size ranging in 36.855 – 47.352 nm, confirming the nano-structured products. This was without the use of any crystal growth inhibitors

(Figure 6a). A beneficial effect was identified when all three parameters were simultaneously set at their high level. All the other combinations either had a non-existent or weakly negative effect on crystallite size (Figure 6b and 6c).

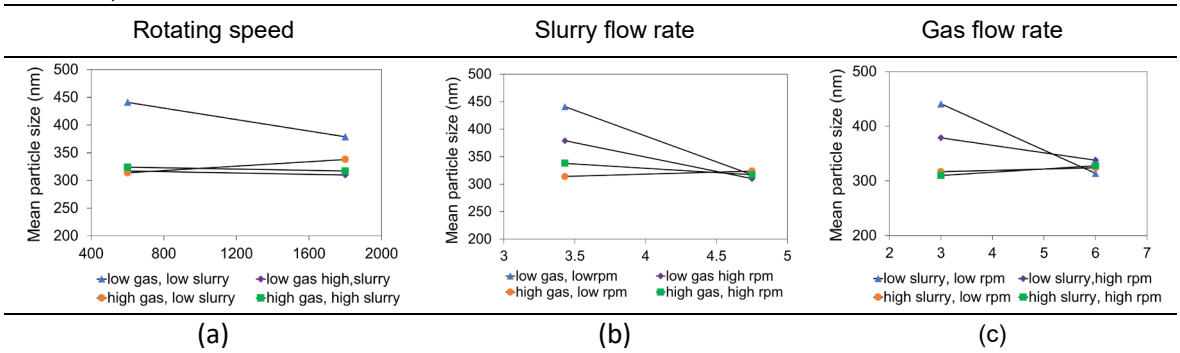

Figure 6. Mean particle size (nm) response incurred by variation of a) rotating speed, b) slurry and c) gas flow. The high and low levels are given in the caption of Figure 4. The sizes were derived from the Image J software

3.3 Process performance on CO_2 capture

Error! Reference source not found. shows the CO_2 capture performance of the RPB pilot plant depending on the L/G ratio and the rotating speed. In all cases the efficiency was higher than 94 %, which was above the 90 % standard efficiency defined for capture processes. Increased L/G ratios are beneficial regardless of rotating speed, while in the case of 1,800 rpm the efficiency is already high, even at lower L/G ratios.

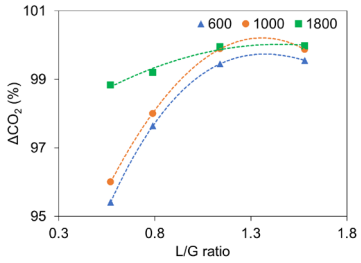

Figure 7. CO_2 capture efficiency (%) of the RPB pilot plant (measurement error ± 1.6 %)

As a general observation it must be noted that the variation of the three operating parameters resulted in trade-offs among the employed KPIs. For example, an increased gas flow rate a) Reduces the residence time of the gas phase inside the RPB, which negatively affected the capture efficiency and reaction yield, but b) at the same time increases the overall mass transfer coefficient, which is desired, because it accelerates the reaction time. There was a triple trade-off between reaction time-product purity-capture efficiency. At low speed (600 rpm) the rotational acceleration was relatively low and most likely not sufficient for handling high flow rates. In this case, the combination of high flows and low rotating speed was responsible for unwanted maldistribution phenomena that reduced the gas-slurry interface (contact area) and obstructed the mass-transfer rate. This translates to increased reaction time, lower ΔCO_2 and/or lower product purity. When the rotational acceleration was sufficient (1800 rpm), high flows were handled well by the RPB and mass transfer was enhanced, due to the improved wetting of the packing material, improved interfacial contact and reduction of mass-transfer resistances, such as liquid film thickness. This is in line with literature (Pan et al., 2015).

4. Conclusions

PCC nanoparticles of primary particle size as low as 181 nm and a crystallite size of 45 nm were successfully produced by slurry carbonation in a pilot scale RPB under mild conditions of temperature and pressure. No crystal growth inhibitors or other additives were applied. No size reduction techniques were employed on the dried product $CaCO_3$ powders. The PSD analysis revealed monodisperses for all operating conditions with the recorded particle sizes being smaller compared to other literature sources employing RPBs (Chang et al., 2012) or conventional equipment (Shirsath et al., 2015). It was proved that RPB enables serious reduction of processing times, overcoming limitations caused by the lower solubility of CO_2 at higher reaction temperatures or Ca ion dissolution rate. Here, simultaneously high values of all control parameters gave the best results in

terms of reaction time. The processing time for 900 g of $Ca(OH)_2$ was approximately halved (49 % reduction), reaching 38 min, when the gas flow rate was appropriately adjusted, with all other operating parameters remaining constant. These remarks seem to agree with other RPB related studies (Chen et al., 2000). The CO_2 capture efficiency remained very high under all applied conditions, reaching 99.9 %. Conditions leading to the reduction of particle size were associated with the co-existence of high slurry flow rates and high rotational speeds (4.75 L/min – 1800 rpm) with a lower gas flow rate (3 L/min).

Nomenclature

$CaCO_3$ – Calcium carbonate
CSTR – Continuously stirred reactor
PCC – Precipitated calcium carbonate
SSA – Specific surface area, m^2/g
V_g – Gas flow rate, L/min
V_{sl} – Slurry flow rate, L/min
T_{rxn} – Reaction temperature, °C
LOI– Loss on ignition 450 - 960 °C, %
PSD- Particle size distribution, nm
$FRCO_2$ – CO_2 feed rate, g CO_2/g solid/h
L/G – Slurry-to-gas ratio
t_{rxn} – Reaction time, min
$\bar{d}$ – Average primary particle size, nm

Acknowledgments

This research has been co-financed by the European Regional Development Fund of the European Union and Greek national funds through the Operational Program Competitiveness, Entrepreneurship and Innovation, under the call RESEARCH – CREATE – INNOVATE (project NANOCAP: T1EDK-02472)

References

Chang E.E., Pan S.Y., Chen Y.H., Tan C.S., Chiang P.C., 2012, Accelerated carbonation of steelmaking slags in a high-gravity rotating packed bed, Journal of Hazardous Materials, 227–228, 97–106.

Chen J.F., Wang Y.H., Guo F., Wang X.M., Zheng C., 2000, Synthesis of nanoparticles with novel technology: High-gravity reactive precipitation, Industrial & Engineering Chemistry Research, 39, 948–954.

Chen Q., Hui T., Sun H., Peng T., Ding W., 2020, Synthesis of magnesium carbonate hydrate from natural talc, Open Chemistry, 18, 951–961.

Chen T.L., Jiang W., Shen A.L., Chen Y.H., Pan S.Y., Chiang P.C., 2020, CO_2 Mineralization and Utilization Using Various Calcium-Containing Wastewater and Refining Slag via a High-Gravity Carbonation Process, Industrial & Engineering Chemistry Research, 59, 7140–7150.

Dimoliani M., Papadopoulos A.I., Seferlis P., 2021, Modelling and Parametric Investigation of Rotating Packed Bed Processes for CO_2 Capture and Mineralisation, Chemical Engineering Transactions, 88, 187–192.

Emami-Meibodi M., Soleimani M., Bani-Najarian S., 2018, Toward enhancement of rotating packed bed (RPB) reactor for $CaCO_3$ nanoparticle synthesis, International Nano Letters, 8, 189–199.

Jimoh O.A., Ariffin K.S., Hussin H. Bin, Temitope A.E., 2018, Synthesis of precipitated calcium carbonate: a review, Carbonates and Evaporites, 33, 331–346.

Kang F., Wang D., Pu Y., Zeng X.F., Wang J.X., Chen J.F., 2018, Efficient preparation of monodisperse $CaCO_3$ nanoparticles as overbased nanodetergents in a high-gravity rotating packed bed reactor, Powder Technology, 325, 405–411.

Neumann K., Gladyszewski K., Groß K., Qammar H., Wenzel D., Górak A., Skiborowski M., 2018, A guide on the industrial application of rotating packed beds, Chemical Engineering Research and Design, 134, 443–462.

Onn M.S., Noh M.G.M., Shukor M.S.M., Isa M.A., 2019, Improving precipitate calcium carbonate (PCC) particle size distribution for a continuous mineral carbonation system, Journal of Physics: Conference Series,1349.

Pan S.Y., Chen Y.H., Chen C. Da, Shen A.L., Lin M., Chiang P.C., 2015, High-Gravity Carbonation Process for Enhancing CO_2 Fixation and Utilization Exemplified by the Steelmaking Industry, Environmental Science and Technology, 49, 12380–12387.

Shirsath S.R., Sonawane S.H., Saini D.R., Pandit A.B., 2015, Continuous precipitation of calcium carbonate using sonochemical reactor, Ultrasonics Sonochemistry, 24, 132–139.

Sun B.C., Wang X.M., Chen J.M., Chu G.W., Chen J.F., Shao L., 2011, Synthesis of nano-$CaCO_3$ by simultaneous absorption of CO_2 and NH_3 into $CaCl_2$ solution in a rotating packed bed, Chemical Engineering Journal, 168, 731–736.

Wang M., Zou H.K., Shao L., Chen J.F., 2004, Controlling factors and mechanism of preparing needlelike $CaCO_3$ under high-gravity environment, Powder Technology, 142, 166–174.